Assessment of the effects of process water recirculation on the surface chemistry and morphology of hydrochar

P. J. Arauzo[1]*, M. P. Olszewski[1], X. Wang[2], J. Pfersich[1], V. Sebastian[3], J. Manyà[4], N. Hedin[2], A. Kruse[1]

* corresponding author: pabloj.arauzo@uni-hohenheim.de

[1]Department of Conversion Technologies of Biobased Resources, Institute of Agricultural Engineering, University of Hohenheim, Garbenstrasse 9, DE-70599 Stuttgart, Germany

[2]Department of Materials and Environmental Chemistry, Stockholm University, SE-10691 Stockholm, Sweden

[3] Department of Chemical Engineering, Aragon Institute of Nanoscience (INA), University of Zaragoza, Campus Río Ebro-Edificio I+D, c/ Poeta Mariano Esquillor s/n, 50018 Zaragoza, Spain

[4]Aragón Institute of Engineering Research (I3A), University of Zaragoza, Crta. Cuarte s/n, Huesca E-22071, Spain

Abstract

The effect of two process water (PW) recirculation strategies after the hydrothermal carbonization (HTC) of brewers spent grains (BSG) is evaluated with the focus on the hydrochar characteristics. The HTC process has been carried out under different operating conditions; residence time between 2 - 4 h and temperature in the range of 200 - 220 °C. The hydrochars composition reveals that operating conditions have a more significant effect than PW recirculation on the hydrochar composition. The composition of the liquid produced at HTC plus PW recirculation process is essentially controlled by the operating temperature, for instance, the total organic carbon (TOC) in the PW changes in the narrow range of 200 - 220 °C. A detailed analysis of PW has also been done. The main components of the liquid phase are lactic, formic, acetic, levulinic, and propionic acid and 5-hydroxymethylfurfural, that affect the surface structure of the hydrochars.

Keywords

Hydrothermal carbonization, Biochar, Aqueous phase, Recirculation, Brewer’s spent grains

1. Introduction

The brewing process requires significant quantities of fresh grain that end up as waste, which leads to an annual world production of approximately 30 million tons of spent grains as by-product [1–3]. However, brewer’s spent grain (BSG) is rich in polysaccharides, proteins and despite the fact of being a widely available and low-cost biomass with nutritional value that can be used for industrial exploitation (e.g. protein source), it is mainly used as animal feed, composted, or disposed as landfill [1,3,4]. Simultaneously, BSG is considered a major biomass resource for energy production through bioconversion processes [5,6]. Therefore, it is necessary to take advantage of this undesired but unavoidable waste material through research and development of new techniques to recover important fractions for the production of a vast range of products.

Hydrothermal carbonization (HTC) is a suitable thermochemical process for the conversion of feedstock with high water content (> 75 wt.%) to produce a solid phase called hydrochar and liquid phase usually called process water (PW). The operation conditions of HTC are temperatures between (180 – 250 °C), reaction time (2 - 12 h), and autogenous pressure (14 - 22 MPa). During the HTC, several types of chemical reactions take place (hydrolysis, dehydration, decarboxylation, polymerization, and aromatization) [7,8] within the feedstock. Hydrochars have several applications in soil amendment, for energy production, and as activated carbon.

Recirculation of PW is also proposed as an economic benefit for the HTC industry, because it is usually necessary to add some initial extra water to have biomass completely soak during the HTC process. The necessity to reduce the quantity of organic matter before the dispose of PW, the cost of initial water and the water treatment of PW thus is saved. A study carried out by Berge et al., [9] showed that PW from HTC of municipal waste streams had high concentration of TOC (total

organic carbon) between 30 and 40 mgL^{-1} and the COD (chemical oxygen demand) was between 60 and 80 mgL^{-1}. PW also contains carboxylic acids, sugars, and furans [10,11]. In addition, a study carried out by Stemann et al. [16] using poplar wood as feedstock concluded that TOC (gL^{-1}) increased after PW recirculation. As consequence of the high amount of TOC in the PW, the major application of PW from different feedstock is anaerobic digestion [12,13]. On the other hand, several studies propose the recirculation of PW in the subsequent HTC as reaction medium to increase the hydrochar yield and improve the physicochemical characteristics of them [14,15]. In fact, several studies show that just the hydrochar yield is increased but that there is no effect on Higher Heating Values (HHV). Uddin et al., [16] studied the effect of different temperatures in the HTC process with PW recirculation using loblolly pine as a feedstock. In their study they found that HHV with and without recirculation of PW were similar.

According to Kruse et al. [17] nitrogen-containing compounds may migrate to the PW with the rise of temperature, due to the hydrolysis reaction mechanism. In the PW nitrogen (N) is found as ammonium (NH_4^+) or nitrates (NO_3^-); furthermore, the ratio of both ions depends on the PW's pH, as ammonium is an acid and nitrate is a weak base.

Barbera et al. [18] studied the nutrient recovery from the PW for the algae cultivation. They evaluated the possibility of the recovery of N and phosphorus (P as phosphate) in hydrochars during the recirculation of PW. The recovery of these macro-nutrients can reduce the energy demand associated with energy supply for fertilizer manufacturing. Due to the protein content of BSG, which is similar to that of algae [19], and the behaviour during HTC [20], similar results to algae studies were expected.

Moreover, there are several studies based on the nitrogen doping in carbon with different nitrogen precursors [21,22]. These sources of nitrogen are usually expensive and non-ecofriendly.

Therefore, the use of initial nitrogen of BSG as green precursor for nitrogen co-doped carbon for applications such as supercapacitors [23] or electrocatalysis [24] is explored.

In this study, the conversion of lignocellulosic biomass rich on protein (BSG) by HTC process with fresh or PW as initial aqueous phase was studied. Even with the knowledge from previous studies which remarked that PW recirculation increase the HHV and hydrochar yield. There is not known previous studies related to a deep research concerning the surface and morphological structure (SE Then, the aims of this study were: i) evaluate the effect in the surface and morphological structure of the hydrochars by the recirculation of PW using feedstock rich in organic nitrogen content ii) a comprehensive comparison of the yield and the physicochemical properties to hydrochar, iii) discussion of the effect of the PW recirculation on the chemical composition of the liquid, iv) recirculation of the PW along HTC process with the purpose of increase the HHV of produced hydrochars for the application as solid fuel.M – EDS, TEM, {1H}13C and 1H NMR spectra).

2. Material and methods

2.1. Material

In this study, brewer's spent grains (BSG) were used as a feedstock, which was provided by Hoepfner Brewery factory (Karlsruhe, Germany), with a moisture content of 78 wt.% and were stored at -15 °C. The elemental analysis (EA) of BSG after it has been dried at 105 °C for 24h were; 49.97 wt.% C, 7.83 wt.% H, 37.48 wt.% O, 3.99 wt.% N, 0.45wt.% S. Proximate analysis (PA) showed the following results (in dry basis), 79.22 wt. % volatile matter (VM), 16.62 wt. % fixed carbon (FC), 4.16 wt.% ash. The HHV of raw BSG, which was calculated using the formula of Channiwala and Parikh [25], was 22.27 MJ kg−1.

2.2. Experimental procedure

In a 250 mL autoclave reactor (stainless steel) 130 g of fresh BSG and 20 g of distilled water or PW were weighed in, respectively. The initial liquid for the first experimental condition was distilled water, while for the second one, the process water (PW) from the first HTC process was used. Finally, for the third one, the PW from the second HTC was used (Figure 1). Afterwards, the closed reactor was placed in a gas-chromatography (GC) oven (Hewlett Packard, GC 5890, Koblenz, Germany) and heated up with a heating rate of (5 °C min^{-1}) until the desired reaction temperature (200 and 220 °C) was reached. The reaction time established for each HTC process was 2 and 4 h. The temperature was measured by a thermocouple, while the pressure was monitored using a digital pressure gauge, each connected with a portable data logger (Endress + Hauseer, RSG30, Nesselwang, Germany). Once the experiment was finished, the reactor was taken out of the oven and quenched in a water bucket for 30 min. When the reactor was cooled down to room temperature, it was moved into a fume hood to release possibly formed gases. The slurry, which was composed of hydrochar and PW, was separated by vacuum filtration using a quantitative filter grade 413 VWR® filter paper (VWR European Cat, Leuven, Germany). First, the hydrochars were dried in an oven at 105 °C for 24 h to ensure complete moisture removal, then they were grinded with a CryoMill (Retsch, Haan, Germany) until a particle size between 150 and 250 µm was accomplished. PW, which were composed of water and dissolved organic compounds, were divided into different containers of which the first one was stored in the fridge at 4 °C to be used on the next recycling. PW for further analysis were frozen at - 24 °C.

Hydrochar and PW obtained from the first HTC process with distilled water, to completely soak the entire biomass and react under homogeneous conditions at different temperature and reaction time, is defined as Reference (Ref). For the subsequent HTC processes (after recirculation of PW),

the samples were defined as Recirculation-1 (Rec-1) and Recirculation-2 (Rec-2), as can also be seen in Figure 1.

2.3. Characterization of solid and liquid phase

Solid phase

The moisture content of the raw BSG and hydrochars were determined according to the DIN EN 14774-3. Furthermore, the VM of raw materials and hydrochars were determined according to DIN 51720:1978-06. The ash content of raw BSG and hydrochars were determined by DIN EN 14775:2010-04, and DIN 51719, respectively. Fixed carbon content was calculated by (Eq. 1, in mass basis)

$$\mathrm{FC}\ (\%) = 100 - \mathrm{Moisture}\ (\%) - \mathrm{VM}\ (\%) - \mathrm{Ash}\ (\%) \quad (1)$$

Elemental analysis was performed using an elemental analyzer (Eurovector S.P.A, Milano, Italy) equipped with a thermal conductivity detector (TCD). Oxygen content was calculated by the difference method (Eq. 2, in mass basis).

$$\mathrm{O}\ (\%) = 100 - \mathrm{C}\ (\%) - \mathrm{H}\ (\%) - \mathrm{N}\ (\%) - \mathrm{S}\ (\%) - \mathrm{Ash}\ (\%) \quad (2)$$

The content of the inorganic elements available in raw biomass and hydrochars of BSG were determined by ICP-OES (Agilent, 720/725-ES emission spectrometer). Morphological analysis of hydrochar samples were carried out by Scanning Electron Microscopy (SEM, Inspect F50; FEI, Eindhoven, the Netherlands) at the LMA-INA-Universidad Zaragoza facilities operated at 10–15 kV. This microscope is equipped with a secondary electron SEM detector ETD (Everhart-Thornley Detector) and an energy-dispersive X-ray microanalysis spectrometer (EDS) to determine the elemental composition and distribution. Both $\{^{1}H\}^{13}C$ and ^{1}H NMR spectra were recorded at frequencies of 100.6 MHz and 400.0 MHz using a Bruker Avance III spectrometer equipped with

a wide-bore magnet (9.4 T), and a 4-mm MAS probe head. Magic angle spinning (MAS) of 14 kHz, ramped crosspolarization (1.5 ms) and SPINAL decoupling of the ^{1}H were used when recording $\{^{1}H\}^{13}C$ NMR spectra. The ^{13}C and ^{1}H chemical shift scales were calibrated externally by using signals of adamantane. For TEM and EELS experiments, powders of each sample was treated by acetone soxhlet extraction for 24 hours to remove the bio oil, and then ultrasonically dispersed in ethanol at room temperature for 2 min and then transferred onto a grid by dipping. Holy carbon coated copper grids were used for both the TEM images and EELS. Transmission electron microscopy (TEM) experiments were performed on a field-emission electron microscope JEOL JEM-2100F, operating at 200 kV. Electron energy-loss spectroscopy (EELS) was performed using a post-column Gatan Image Filter (GIF Tridium).

Liquid

The pH values of PW of the liquid samples were measured using a HACH HQ40d multi equipment. A Shimadzu TOC Analyzer 5050A was used to determine the TOC of PW. PW of HTC includes high value molecules (lactic acid, formic acid, acetic acid, levulinic acid, propionic acid, HMF, and furfural) which were determined using a HPLC device (Shimadzu 20AD, Shimadzu, Japan). It is equipped with a column (HPX-87H), UV-Vis detector (SPD-20A, Shimadzu, Japan), and refractive index detector (RID-10A, Shimadzu, Japan).

2.4. Calculations

The yield of hydrochar (Hy, wt.%) was calculated according to Eq.3, whereas the HHV was calculate following the equation of Channiwala and Parikh [25] for each recirculation.

$$Hy(wt.\%) = \frac{mass\ of\ dried\ hydrochar}{mass\ of\ total\ dried\ feedstock} * 100; \quad (3)$$

$$FR = \frac{Fixed\ Carbon}{Volatile\ matter}; \quad (4)$$

3. Results and discussion

3.1. Effects on the yield of hydrochar

Table 1 shows the pressure achieved in the autoclave after the reaction time at the desired temperature (° C) and the pH of the PW, after filtration of the resulting slurry. In order to ensure the reproducibility of the results, all experiments were repeated in triplicate. The pH was in acidic range and slightly decreased after the recirculation, because of released organic acids from the biomass [26]. An assumption for the reason of obtaining the most basic value of pH at 220 °C might be the higher release of organic compounds to PW and the degradation of organic acids during HTC [27]. The hydrochar yield (Hy, wt.%) (Table 1) obtained after 2 h was larger than at 4 h, which can be due to the higher degree of decomposition caused by the hydrolysis of cellulose [28]. In Table 1, two different trends could be observed. First, after PW recirculation at 200 °C the Hy (wt.%) decreased with one PW recirculation and then increases again, while; second, at 220 °C the opposite effect was observed. The latter was previously observed in a study carried out by Reza et al., [29].

The presence of organic acids (lactic, acetic, and formic) in the PW produced during the first HTC experiments and used in the subsequent HTC might have a catalytic effect during the hydrolysis of cellulose [30,31]. Formation of intermediates (i.e. 5-hydroxymethylfurfural and furfural) released from the hexoses and pentoses, both initially found in the biomass, can also explain the trend of Hy (wt.%) (Table 1) and C (wt.%) (Table 4) after two PW recirculation. The intermediates are accumulated in the PW can lead to the formation of secondary char [32], which can also be produced through polymerization reactions during the HTC process [33]. This seems to be

confirmed by the relatively sharp increase in the TOC values after the first recirculation at 220 °C (Table 2) due to the accumulation of water soluble compounds, such as sugars, organic acids, and other organic compounds in the PW[33]. However, at 200 °C the TOC decreased after each HTC process, probably as a consequence of the incomplete hydrolysis of the cellulose [11,16].

Figure 2 shows the relationship between the yield of hydrochar and the HHV. The values of HHV were slightly higher at high temperatures but the recirculation of PW does not enhance the HHV at the same temperature and reaction time. No effect by using PW in the subsequent HTC processes on the HHV was previously reported in earlier studies [11,16]. The increase in the yield of 5-hydroxymethylfurfural (HMF) found at 220 °C (Table 2), which has a HHV of 22.2 MJ/kg, can be an explanation for this effect [34].

3.2. Effects on proximate and elemental composition of biochars

Dry matter content, VM, ash, and FC for raw biomass and hydrochars were determined in four repetitions summarized in Table 3. As expected, the highest VM was found in the raw biomass at 79.2 wt. %. For resulting hydrochars, the lowest value of VM (64.0 wt. %) was measured when the HTC process was conducted at 220 °C, a reaction time of 4 h and without PW recirculation. This means that 19.3 wt. % of the initial VM was removed from the feedstock towards the PW. In comparison with the hydrochar produced at the lowest temperature (200 °C) and 2 h reaction time without PW recirculation, the reduction was 8.5 %. According to the findings of Wu et al., [35] the VM from biomass feedstock are mainly composed of oxygenated organics like aldehydes, ketones, esters, acids, furans, saccharides, and phenols. An increased temperature can promote the migration of these compounds to the PW (especially for sugars and acids). Regardless of the HTC operating conditions, the first recirculation of PW led to a decrease in the VM of resulting

hydrochar, except for the experiment conducted at the highest severity (220 °C for 4 h of reaction time).

From the raw BSG to the hydrochar obtained at 220 °C and a reaction time of 4 h without recirculation, the FC content increased 1.9 times. The coalification process leads to a decrement of VM because of the migration from the solid to the liquid phase [20] and a subsequent increase in the FC during HTC. Furthermore, the coalification process increased with the reaction severity which, in table 2, is represented as the fuel ratio (Eq. 4). The fuel ratio (FR) of hydrochar obtained at 220 °C and 4 h reaction time is 2.3 times higher than that of raw biomass. This also means 0.7 times higher than the hydrochar produced at 200 °C and 2 h reaction time.

Table 4 shows the results from the elemental analysis of the raw material and hydrochars obtained at different operating conditions. The recirculation of PW during HTC produced an increase of the nitrogen content in the hydrochar. At 220 °C, 4 h reaction time and after the first recirculation of PW the maximum carbon content was obtained with 67.7 wt.%, which is 1.3 times higher than that of raw biomass. At the same conditions, the highest content of hydrogen was also attained (8.3 wt. %). The C/N ratio of hydrochars decreased with the recirculation of PW, except for the experiments performed at 220 °C and 2 h, which present an opposite tendency. A decrement of the C/N ratio means that the N content increases with recirculation. This can be explained by the migration of nitrogen compounds (e.g. amines) to the liquid phase at higher temperatures [17]. A study carried out by Bargmann et al. [36] found similar values of C/N ratios of BSG-derived hydrochars; however, they found an opposite behavior for the increment of residence time. Compared to the typical C/N ratios of charcoal [37], the ones obtained were smaller. Low C/N ratios and the assumption of a high mineral N content in the hydrochars enables the possibility to be used as fertilizer [36]. The Hydrogen content increased after two recirculation at 200 °C and one recirculation at 220 °C independently of the reaction time, while the oxygen content decreased by

41.5 % compared to the raw feedstock with the lowest temperature (200 °C) and reaction time of 2 h. With applied operating conditions of 220 °C and 4 h reaction time, the decrease of oxygen content by 51.3 % therefore is bigger. This confirmed that the deoxygenation reactions take place during the HTC [8].

Table 4 also reports the O/C and H/C atomic ratios, which decreased after HTC. More in detail both the O/C and H/C atomic ratios from raw biomass converted to the hydrochar obtained after HTC at 200 °C for 4 h and one PW recirculation decreased by 64.3 % and 22.3 %, respectively. As can be seen from the Van Krevelen diagram in Figure 3, there was no notable difference in the O/C and H/C atomic ratios for different hydrochars produced at different operating conditions. In other words, recirculation of PW did not lead to further decarboxylation and dehydration reactions [11,33].

The raw BSG consisted of 43.0 wt. % hemicellulose [20], which is mainly composed of sugar molecules exhibiting a high oxygen content. The hydrolysis of the hemicellulose, which starts at 180 °C [38], and the consecutive dehydration can explain the reduction of O/C atomic ratios in hydrochars. This is due to the fact that cellulose has a higher degree of crystallinity as well as more organized structure than hemicellulose. Thus, glycosidic bonds in the hemicellulose are more accessible than the ones from crystalline cellulose [39]. During HTC, an increase of temperature resulted in the decline of O/C and H/C atomic ratios because cellulose starts to be decomposed at 200 °C *via* dehydration and decarboxylation reactions [8]. Sugars formed by these reactions and further released from hemicellulose react to HMF and furfurals by elimination of water. This is the most important reaction in view of the reduction of the oxygen content [40]. Furthermore, water is eliminated during polycondensation of the furfurals, leads to a lower impact of oxygen content [40]. In principle, the same happens with cellulose, but especially crystalline cellulose is stabilized by hydrogen bonds, which hydrolyses at higher temperature than hemicellulose. Moreover, CO_2

elimination becomes more important at higher temperatures [20]. Due to the relatively narrow range of operating conditions (200 °C, 220 °C, 2 h, 4h) analyzed here, the O/C and H/C atomic ratios plotted on the Van Krevelen diagram (Figure 3) are in the range of lignite.

Table 5 shows the main inorganic elements present in the raw biomass and the produced hydrochars. In the produced hydrochars, higher amounts of calcium salts were found in comparison to the raw biomass. The mass fraction of the elements iron, manganese and potassium in the hydrochars are larger than in raw biomass. However, the increase of the mass fraction of the elements is not constant during the recirculation of PW. A study carried by Reza et al., [29] used herbaceous and agricultural biomass as initial feedstock and proved that some alkali and alkaline compounds can be leached from the structure of the biomass. Thus, it is possible that during HTC, the aqueous media could become saturated of inorganic elements during the first recirculation of PW. Therefore, the inorganic elements might migrate from the saturated aqueous phase to the hydrochar during the second recirculation of PW.

3.3. Effects on the surface morphology

Depending on the HTC operating conditions and PW recirculation, the surface of the hydrochar dramatically changed (Figure 4). The SEM images of the hydrochars at 24000x magnification show that for hydrochars produced at the lowest temperature (200 °C) after 2 and 4 h reaction time, the recirculation of PW had no effect on their morphological features, which can also be seen by comparing the TEM results. These low-temperature hydrochars clearly retained the porous structure of raw biomass [41]. This may be due to the fact that the cellulose structure is not completely decomposed. TEM images (Figure 4) corroborate this effect, showing that hydrochar starts to rise in the area previously occupied by cellulose. The raise of the operating temperature from 200 °C to 220 °C has an effect on the surface of the hydrochars promoting the formation of

micro-size spheres. In addition, 13C-NMR and 1H- NMR figures show the unreacted cellulose after HTC. A study carried out by Titirici et al. [42] found a similar effect in the surface of the hydrochars produced by using carbohydrates (e.g. D(+)-Glucose, D(+)-xylose, D(+)-maltose monohydrate) and HMF as starting material. The transformation of the surface of the hydrochars may be due to the secondary char reactions by the sugars (carbohydrates) and acids contained in the PW (Table 2). Secondary char formation can be confirmed by the increment of the C/O atomic ratios on the surface of the hydrochars (Table 6). Electron energy loss spectroscopy (EELS) was used to determine the fraction of sp^2/sp^3 carbon of the hydrochars by analyzing the near-edge fine structure of the carbon ionization edge, based on the method of Urbonaite et al. [43], Jeanne-Rose et al., [44]. The feature at ~285 eV is due to a transition of a 1s electron to the π* antibonding orbital, and the next 20 eV mainly contains features due to transitions from 1s to σ* states, and the sp^2/sp^3 intensity ratios of these curves have been shown to be related to the hybridization of the carbon atoms [45]. The π*/σ* intensity ratios are similar, indicating that these hydrochars after PW recirculation have similar fraction of sp^2/sp^3 carbon after. The statistical deviation is ±0.02 by using this approach [46]. In addition, the hydrolysis of proteins to amines during HTC also has an effect regarding the surface of the hydrochars [47].Then, the changes observed on the surface of the produced hydrochars may be a combination of factors: severity of the reaction, the secondary char formation, and hydrolysis of proteins.

3.4. Effects on the surface composition

Table 6 also reveals the presence of inorganic elements (K, Si, P, S, Ca) in the PW recirculation. The above-mentioned increase in the C/O atomic ratio in the surface of hydrochars is in good agreement with the micro-size sphere formation shown in SEM-images. The microspheres are condensation products from furfurals, which have a relatively low oxygen content. On the other hand, the EDX technique cannot detect N due to the overlapping of its energy with other elements.

The changes in the composition of hydrochar on surface by recirculation of PW are related to the reactions between the compounds available in the PW and those present in the fresh feedstock. Usually, acids are formed during HTC; however, during water recirculation, acids are present from the beginning of the reaction. This should increase the reaction rate especially of the hydrolysis and thus might explain the increase in TOC by water recirculation at 220°C (Table 2). At 200°C, the TOC content decreases, especially after the first recirculation. Furthermore, the formation of the secondary char is incomplete at this comparatively low temperature. This is also visible in SEM-images, which shows low formation of spheres at this temperature. In this case, the low input of e.g. HMF forces the polymerization. Moreover, the different dependences of hydrolysis and its consecutive reaction, the polymerization, on acidic catalysis and temperature can be seen. According to the findings found by Körner et al. [48] the hydrolysis is more sensitive to pH than the polymerization. In this case, the pH at the beginning is more important than the pH after the reaction, which is only slightly increasing (Table 1). This is in good agreement with observations done by previous researchers [15,33].

3.5. Effects on the acid content in the liquid phase

From the results listed in Table 2, it is also observed that the increase in acid content in the PW after the PW recirculation was not as high as the first HTC with fresh water. Körchemann et al., [49] found that after several recirculation cycles the acid content of the PW stays nearly constant. However, the reason for this behaviour was not discussed. We suggest different hypothesis for explaining this finding. One approach is that a reverse reaction, which builds HMF or furfurals out of acids is quite hard to expect due to the endothermic pathway of building a new bond, which is unfavorable at high temperatures. This is also the reason for the equilibrium to be forced to the acid side of the reaction equation. Another explanation would be a reaction of the acids with some other compound in the PW or of the biomass. Both explanations together with the information of

Körchemann et al., [49] would mean that at 180 °C or 200 °C, the reaction of acids with other compounds is slower than the reaction of HMF and furfurals to acids until a certain concentration is reached. This explanation seems to be supported by the fact that, at a higher acid concentration, the hydrolysis of the biomass is catalyzed, thus leading to newly formed compounds attached to the surface of the char.

Due to a huge amount of different compounds in the PW after some recirculation steps the effects occurring in between these compounds get harder and harder to describe and proof, as get the disclosure of the actually present compounds. Some kind of precipitation or incorporation in the char could be the result, as well as an adsorption in the pores of the char. The latter one could be easily found out by comparing the concentration of released acids from the chars after washing the char of the first step and the following ones.

4. Conclusions

The recirculation of PW at the HTC process effect the proximate composition of the hydrochars produced. This is due to changes on the reaction pathways under different operating conditions as; PW composition, pH, and the presence of inorganics. It has been determined that the first PW recirculation is the most effective. The surface morphology images, of the produced hydrochars, show that it is affected by the polymerization of intermediates from process water recirculation. Recirculation of PW after the HTC process is suitable for the reduction of process water and the amount of water used in total, in hydrothermal carbonization processes.

Appendix A. Supplementary data

E-supplementary data of this work can be found in online version of the paper

Funding

This research was funded by the European Union's Horizon 2020 research and innovation program under the Marie Skłodowska-Curie Grant Agreement No. 721991 and Deutsche Forschungsgemeinschaft (DFG, German Research Foundation) – 328017493/GRK 2366 (International Research Training Group "Adaption of maize-based food-feed-energy systems to limited phosphate resources").

Acknowledgments

We gratefully acknowledge the work of doctoral candidate Ekatarina Ovsyannikova for ICP-OES measurements and Andre Bendana for his support conducting experiments. The authors would like to thank Prof. Gunnar Svensson for the valuable discussions concerning the TEM/EELS analyses.

Table 1. Operating conditions of the HTC processes: reaction temperature (*T*), reaction time (*t*), pH and hydrochar yield (standard deviation with two replications).

Sample	*T* [°C]	*t* [h]	*p* [bar]	pH	Hy [%]
200-2h-Ref	200	2	23.20 ± 0.40	4.47 ± 0.00	58.99 ± 0.98
200-2h-Rec-1	200	2	23.50 ± 1.40	4.45 ± 0.06	51.78 ± 0.46
200-2h-Rec-2	200	2	23.90 ± 0.10	4.34 ± 0.08	60.36 ± 1.06
200-4h-Ref	200	4	24.10 ± 0.50	4.57 ± 0.06	54.62 ± 0.15
200-4h-Rec-1	200	4	23.35 ± 0.25	4.56 ± 0.04	48.22 ± 0.34
200-4h-Rec-2	200	4	25.45 ± 0.55	4.46 ± 0.04	51.32 ± 0.97
220-2h-Ref	220	2	35.55 ± 0.05	4.59 ± 0.13	56.03 ± 0.89
220-2h-Rec-1	220	2	37.25 ± 0.95	4.55 ± 0.06	55.22 ± 0.25
220-2h-Rec-2	220	2	35.20 ± 1.00	4.48 ± 0.07	70.25 ± 0.42
220-4h-Ref	220	4	38.20 ± 2.30	4.70 ± 0.00	65.86 ± 0.53
220-4h-Rec-1	220	4	38.85 ± 1.95	4.53 ± 0.10	54.19 ± 0.41
220-4h-Rec-2	220	4	37.50 ± 1.00	4.51 ± 0.02	55.18 ± 0.64

Table 2. Yield of different compounds in the liquid phase and total organic content (standard deviation with two replications)

Sample Name	Yield to compounds into liquid phase (wt. %)						TOC [g L^{-1}]
	Lactic acid	Formic acid	Acetic acid	Levulinic acid	Propionic acid	HMF	
200-2h-Ref	0.82 ± 0.01	1.05 ± 0.13	1.76 ± 0.06	0.25 ± 0.01	5.01 ± 0.26	0.04 ± 0.00	16.99
200-2h-Rec-1	0.84 ± 0.04	0.96 ± 0.04	1.69 ± 0.07	0.22 ± 0.06	4.98 ± 0.10	0.05 ± 0.01	14.88
200-2h-Rec-2	1.01 ± 0.05	2.34 ± 0.05	2.20 ± 0.05	0.36 ± 0.05	5.07 ± 0.05	0.04 ± 0.01	15.09
200-4h-Ref	1.30 ± 0.09	1.65 ± 0.16	1.80 ± 0.16	0.34 ± 0.02	4.66 ± 0.30	0.05 ± 0.00	21.82
200-4h-Rec-1	1.53 ± 0.12	1.80 ± 0.06	2.06 ± 0.12	0.38 ± 0.05	5.24± 0.26	0.08 ± 0.01	17.71
200-4h-Rec-2	1.47 ± 0.07	1.68 ± 0.04	1.96 ± 0.05	0.34 ± 0.01	5.16 ± 0.23	0.07 ± 0.01	12.40
220-2h-Ref	1.67 ± 0.09	1.57 ± 0.07	2.26 ± 0.04	0.41 ± 0.01	5.65 ± 0.13	0.09 ± 0.00	15.61
220-2h-Rec-1	1.91 ± 0.07	1.66 ± 0.08	2.57 ± 0.04	0.45 ± 0.01	6.48 ± 0.28	0.11 ± 0.00	17.76
220-2h-Rec-2	2.06 ± 0.12	2.06 ± 0.13	2.81 ± 0.06	0.49 ± 0.02	6.17± 0.00	0.11 ± 0.01	28.52
220-4h-Ref	2.21 ± 0.04	1.72 ± 0.06	2.76 ± 0.08	0.53 ± 0.02	7.01 ± 0.05	0.12 ± 0.01	14.89
220-4h-Rec-1	2.14 ± 0.17	0.95 ± 0.00	2.64 ± 0.17	0.49 ± 0.02	7.41 ± 0.01	0.17 ± 0.06	17.40
220-4h-Rec-2	1.78 ± 0.12	1.07 ± 0.20	2.10 ± 0.01	0.39 ± 0.01	5.99 ± 0.10	0.11 ± 0.02	20.36

Table 3. Proximate analysis and Fuel ratio of produced hydrochars (standard deviation with four replications).

Sample	Proximate Analysis dry basis [wt.%]			Fuel ratio
	VM	Ash	FC	
Raw	79.22 ± 0.00	4.16 ± 0.00	16.62 ± 0.00	0.21
HTC-200-2h-Ref	70.70 ± 0.55	4.52 ± 0.04	24.78 ± 0.51	0.35
HTC-200-2h-Rec-1	69.28 ± 0.03	3.81 ± 0.11	26.91 ± 0.14	0.39
HTC-200-2h-Rec-2	70.69 ± 0.27	4.11 ± 0.04	25.20 ± 0.23	0.36
HTC-200-4h-Ref	69.46 ± 0.30	4.71 ± 0.24	25.83 ± 0.06	0.37
HTC-200-4h-Rec-1	67.55 ± 0.13	4.93 ± 0.21	27.52 ±0.09	0.41
HTC-200-4h-Rec-2	69.32 ±0.24	4.65 ± 0.43	26.02 ± 0.19	0.38
HTC-220-2h-Ref	66.32 ± 0.13	4.08 ± 0.14	29.60 ± 0.27	0.45
HTC-220-2h-Rec-1	65.81 ± 0.30	4.63 ± 0.30	29.55 ± 0.60	0.45
HTC-220-2h-Rec-2	66.62 ± 0.54	4.43 ± 0.06	28.94 ± 0.48	0.43
HTC-220-4h-Ref	63.95 ± 0.23	4.63 ± 0.18	31.42 ± 0.05	0.49
HTC-220-4h-Rec-1	66.91 ± 0.07	4.35± 0.25	28.74 ± 0.18	0.43
HTC-220-4h-Rec-2	64.86 ± 0.17	4.55 ± 0.21	30.60 ± 0.04	0.47

Table 4. Elemental Analysis, O/C and H/C atomic ratios, C/N ratio and Higher Heating Value (MJ/kg) of the hydrochars (standard deviation with four replications).

	EA db [wt.%]					Atomic			
Sample	N %	C %	H %	S %	O %	O/C	H/C	C/N	HHV[MJ/kg]
Raw	3.99 ± 0.00	49.97 ± 0.05	7.83 ± 0.06	0.45 ± 0.01	33.59 ± 0.11	0.56	1.88	12.52	23.10
HTC-200-2h-Ref	3.75 ± 0.05	61.87 ± 0.44	7.98 ± 0.18	0.60 ± 0.02	21.28 ± 0.55	0.26	1.55	16.49	28.71
HTC-200-2h-Rec-1	3.91 ± 0.05	60.64 ± 0.14	7.65 ± 0.08	0.60 ± 0.01	23.40 ± 0.10	0.29	1.51	15.53	27.68
HTC-200-2h-Rec-2	3.99 ± 0.10	60.80 ± 0.23	7.72 ± 0.10	0.59 ± 0.02	22.80 ± 0.45	0.25	1.52	15.24	27.87
HTC-200-4h-Ref	3.88 ± 0.08	62.49 ± 0.24	7.55 ± 0.38	0.60 ± 0.02	20.78 ± 0.71	0.26	1.45	16.11	28.46
HTC-200-4h-Rec-1	3.95 ± 0.06	61.71 ± 0.26	7.49 ± 0.02	0.58 ± 0.01	21.35 ± 0.35	0.24	1.46	15.62	28.05
HTC-200-4h-Rec-2	4.04 ± 0.09	62.68 ± 0.22	7.91 ± 0.01	0.60 ± 0.01	20.12 ± 0.33	0.23	1.51	15.54	29.03
HTC-220-2h-Ref	4.09 ± 0.10	64.12 ± 0.54	7.72 ± 0.06	0.58 ± 0.02	19.40 ± 0.56	0.20	1.45	15.67	29.39
HTC-220-2h-Rec-1	4.15 ± 0.04	65.17 ± 0.47	8.13 ± 0.00	0.63 ± 0.01	17.29 ± 0.51	0.20	1.50	15.71	30.45
HTC-220-2h-Rec-2	3.98 ± 0.10	63.73 ± 0.00	7.65 ± 0.34	0.56 ± 0.00	19.64 ± 0.23	0.23	1.44	16.02	29.14
HTC-220-4h-Ref	4.09 ± 0.07	65.52 ± 0.34	8.05 ± 0.26	0.54 ± 0.00	17.18 ± 0.63	0.20	1.47	16.03	30.47
HTC-220-4h-Rec-1	4.27 ± 0.04	67.69 ± 0.26	8.26 ± 0.03	0.60 ± 0.01	14.83 ± 0.18	0.16	1.46	15.87	31.73
HTC-220-4h-Rec-2	4.12 ± 0.01	65.33 ± 0.03	8.19 ± 0.13	0.60 ± 0.02	17.22 ± 0.22	0.20	1.50	15.87	30.58

Table 5. Inorganic elements found in the hydrochars by means of ICP-OES.

Sample	Inorganic elements [mg/g]					
	Ca	Fe	K	Mg	Mn	P
Raw	3.29	0.08	n.d.	2.21	0.01	4.88
HTC-200-2h-Ref	6.79	0.18	< 0.36	1.86	0.06	5.53
HTC-200-2h-Rec-1	4.57	0.13	< 0.36	1.47	0.03	4.08
HTC-200-2h-Rec-2	7.45	0.19	< 0.36	2.23	0.06	6.42
HTC-200-4h-Ref	4.56	0.15	< 0.36	1.35	0.04	3.91
HTC-200-4h-Rec-1	6.09	0.17	< 0.36	2.02	0.05	5.54
HTC-200-4h-Rec-2	5.49	0.16	< 0.36	1.92	0.05	4.98
HTC-220-2h-Ref	5.93	0.19	< 0.36	1.67	0.05	4.92
HTC-220-2h-Rec-1	5.81	0.16	< 0.36	1.82	0.04	5.00
HTC-220-2h-Rec-2	6.26	0.17	< 0.36	1.93	0.05	5.40
HTC-220-4h-Ref	6.13	0.17	< 0.36	1.78	0.05	5.22
HTC-220-4h-Rec-1	6.02	0.19	< 0.36	2.12	0.05	5.40
HTC-220-4h-Rec-2	4.95	0.17	< 0.36	1.66	0.04	4.52

Table 6. EDX elemental analysis of produced hydrochars and C/O atomic ratio.

Sample	Elements measured by EDX [wt. %]					Atomic ratio
	C	O	P	Ca	S	C/O
200-2h-Ref	69.50	29.34	0.47	0.41	0.28	3.16
200-2h-Rec-1	76.52	22.78	0.04	0.05	0.61	4.48
200-2h-Rec-2	76.41	22.24	0.51	0.43	0.40	4.58
200-4h-Ref	75.47	23.57	0.36	0.45	0.14	4.27
200-4h-Rec-1	76.75	22.62	0.19	0.22	0.22	4.52
200-4h-Rec-2	75.88	22.21	0.68	0.93	0.29	4.55
220-2h-Ref	76.53	23.07	0.05	0.08	0.27	4.42
220-2h-Rec-1	77.57	21.98	0.15	0.15	0.15	4.71
220-2h-Rec-2	79.35	19.89	0.39	0.08	0.29	5.32
220-4h-Ref	77.43	21.77	0.24	0.32	0.23	4.74
220-4h-Rec-1	76.65	22.63	0.22	0.29	0.20	4.52
220-4h-Rec-2	76.78	22.96	0.08	0.09	0.09	4.46

References

[1] S. Ikram, L. Huang, H. Zhang et al., “Composition and Nutrient Value Proposition of Brewers Spent Grain,” *Journal of food science*, vol. 82, no. 10, pp. 2232–2242, 2017.

[2] A. Montusiewicz, S. Pasieczna-Patkowska, M. Lebiocka et al., “Hydrodynamic cavitation of brewery spent grain diluted by wastewater,” *Chemical Engineering Journal*, vol. 313, pp. 946–956, 2017.

[3] R. Ravindran, S. Jaiswal, N. Abu-Ghannam et al., “A comparative analysis of pretreatment strategies on the properties and hydrolysis of brewers’ spent grain,” *Bioresource Technology*, vol. 248, pp. 272–279, 2018.

[4] S. Spinelli, A. Conte, L. Lecce et al., “Supercritical carbon dioxide extraction of brewer's spent grain,” *The Journal of Supercritical Fluids*, vol. 107, pp. 69–74, 2016.

[5] I. Celus, K. Brijs, and J. A. Delcour, “Fractionation and characterization of brewers' spent grain protein hydrolysates,” *Journal of agricultural and food chemistry*, vol. 57, no. 12, pp. 5563–5570, 2009.

[6] E. Vieira, M. A. M. Rocha, E. Coelho et al., “Valuation of brewer's spent grain using a fully recyclable integrated process for extraction of proteins and arabinoxylans,” *Industrial Crops and Products*, vol. 52, pp. 136–143, 2014.

[7] A. Kruse, A. Funke, and M.-M. Titirici, “Hydrothermal conversion of biomass to fuels and energetic materials,” *Current opinion in chemical biology*, vol. 17, no. 3, pp. 515–521, 2013.

[8] A. Funke and F. Ziegler, “Hydrothermal carbonization of biomass: A summary and discussion of chemical mechanisms for process engineering,” *Biofuels, Bioproducts and Biorefining*, vol. 4, no. 2, pp. 160–177, 2010.

[9] N. D. Berge, K. S. Ro, J. Mao et al., “Hydrothermal carbonization of municipal waste streams,” *Environmental science & technology*, vol. 45, no. 13, pp. 5696–5703, 2011.

[10] S. K. Hoekman, A. Broch, and C. Robbins, “Hydrothermal Carbonization (HTC) of Lignocellulosic Biomass,” *Energy & Fuels*, vol. 25, no. 4, pp. 1802–1810, 2011.

[11] B. Weiner, J. Poerschmann, H. Wedwitschka et al., “Influence of Process Water Reuse on the Hydrothermal Carbonization of Paper,” *ACS Sustainable Chemistry & Engineering*, vol. 2, no. 9, pp. 2165–2171, 2014.

[12] B. Wirth and J. Mumme, “Anaerobic Digestion of Waste Water from Hydrothermal Carbonization of Corn Silage,” *Applied Bioenergy*, vol. 1, 2013.

[13] I. Oliveira, D. Blöhse, and H.-G. Ramke, “Hydrothermal carbonization of agricultural residues,” *Bioresource Technology*, vol. 142, pp. 138–146, 2013.

[14] X. Chen, X. Ma, X. Peng et al., “Effects of aqueous phase recirculation in hydrothermal carbonization of sweet potato waste,” *Bioresource Technology*, vol. 267, pp. 167–174, 2018.

[15] J. Stemann, A. Putschew, and F. Ziegler, “Hydrothermal carbonization: Process water characterization and effects of water recirculation,” *Bioresource Technology*, vol. 143, pp. 139–146, 2013.

[16] M. H. Uddin, M. T. Reza, J. G. Lynam et al., “Effects of water recycling in hydrothermal carbonization of loblolly pine,” *Environmental Progress & Sustainable Energy*, vol. 34, n/a-n/a, 2013.

[17] A. Kruse, F. Koch, K. Stelzl et al., “Fate of Nitrogen during Hydrothermal Carbonization,” *Energy & Fuels*, vol. 30, no. 10, pp. 8037–8042, 2016.

[18] E. Barbera, A. Bertucco, and S. Kumar, “Nutrients recovery and recycling in algae processing for biofuels production,” *Renewable and Sustainable Energy Reviews*, vol. 90, pp. 28–42, 2018.
[19] D. Chiaramonti, M. Prussi, M. Buffi et al., “Review and experimental study on pyrolysis and hydrothermal liquefaction of microalgae for biofuel production,” *Applied Energy*, vol. 185, pp. 963–972, 2017.
[20] P. Arauzo, M. Olszewski, and A. Kruse, “Hydrothermal Carbonization Brewer’s Spent Grains with the Focus on Improving the Degradation of the Feedstock,” *Energies*, vol. 11, no. 11, p. 3226, 2018.
[21] S. Yang, X. Feng, X. Wang et al., “Graphene-based carbon nitride nanosheets as efficient metal-free electrocatalysts for oxygen reduction reactions,” *Angewandte Chemie (International ed. in English)*, vol. 50, no. 23, pp. 5339–5343, 2011.
[22] R. Liu, D. Wu, X. Feng et al., “Nitrogen-doped ordered mesoporous graphitic arrays with high electrocatalytic activity for oxygen reduction,” *Angewandte Chemie (International ed. in English)*, vol. 49, no. 14, pp. 2565–2569, 2010.
[23] Y. Shao, S. Zhang, M. H. Engelhard et al., “Nitrogen-doped graphene and its electrochemical applications,” *Journal of Materials Chemistry*, vol. 20, no. 35, p. 7491, 2010.
[24] Z. Mo, S. Liao, Y. Zheng et al., “Preparation of nitrogen-doped carbon nanotube arrays and their catalysis towards cathodic oxygen reduction in acidic and alkaline media,” *Carbon*, vol. 50, no. 7, pp. 2620–2627, 2012.
[25] S. A. Channiwala and P. P. Parikh, “A unified correlation for estimating HHV of solid, liquid and gaseous fuels,” *Fuel*, vol. 81, no. 8, pp. 1051–1063, 2002.
[26] H. Wallman, *Laboratory studies of a hydrothermal pretreatment process for municipal solid waste*, 1995.
[27] B. M. Ghanim, D. S. Pandey, W. Kwapinski et al., “Hydrothermal carbonisation of poultry litter: Effects of treatment temperature and residence time on yields and chemical properties of hydrochars,” *Bioresource Technology*, vol. 216, pp. 373–380, 2016.
[28] X. Zhao, G. C. Becker, N. Faweya et al., “Fertilizer and activated carbon production by hydrothermal carbonization of digestate,” *Biomass Conversion and Biorefinery*, vol. 8, no. 2, pp. 423–436, 2018.
[29] M. T. Reza, J. G. Lynam, M. H. Uddin et al., “Hydrothermal carbonization: Fate of inorganics,” *Biomass and Bioenergy*, vol. 49, pp. 86–94, 2013.
[30] U. Ekpo, A. B. Ross, M. A. Camargo-Valero et al., “Influence of pH on hydrothermal treatment of swine manure: Impact on extraction of nitrogen and phosphorus in process water,” *Bioresource Technology*, vol. 214, pp. 637–644, 2016.
[31] X. Lu, J. R. V. Flora, and N. D. Berge, “Influence of process water quality on hydrothermal carbonization of cellulose,” *Bioresource Technology*, vol. 154, pp. 229–239, 2014.
[32] M. Volpe and L. Fiori, “From olive waste to solid biofuel through hydrothermal carbonisation: The role of temperature and solid load on secondary char formation and hydrochar energy properties,” *Journal of Analytical and Applied Pyrolysis*, vol. 124, pp. 63–72, 2017.
[33] A. Kabadayi Catalkopru, I. C. Kantarli, and J. Yanik, “Effects of spent liquor recirculation in hydrothermal carbonization,” *Bioresource Technology*, vol. 226, pp. 89–93, 2017.

[34] S. P. Verevkin, V. N. Emel'yanenko, E. N. Stepurko et al., "Biomass-Derived Platform Chemicals: Thermodynamic Studies on the Conversion of 5-Hydroxymethylfurfural into Bulk Intermediates," *Industrial & Engineering Chemistry Research*, vol. 48, no. 22, pp. 10087–10093, 2009.
[35] K. Wu, Y. Gao, G. Zhu et al., "Characterization of dairy manure hydrochar and aqueous phase products generated by hydrothermal carbonization at different temperatures," *Journal of Analytical and Applied Pyrolysis*, vol. 127, pp. 335–342, 2017.
[36] I. Bargmann, M. C. Rillig, A. Kruse et al., "Effects of hydrochar application on the dynamics of soluble nitrogen in soils and on plant availability," *Journal of Plant Nutrition and Soil Science*, vol. 177, no. 1, pp. 48–58, 2014.
[37] P. Pinwisat, S. Phoolphundh, S. Buddhawong et al., "Effect of Surfactant-Coated Charcoal Amendment on the Composting Process and Nutrient Retention," *Environmental Engineering Research*, vol. 19, no. 1, pp. 37–40, 2014.
[38] J. A. Libra, K. S. Ro, C. Kammann et al., "Hydrothermal carbonization of biomass residuals: A comparative review of the chemistry, processes and applications of wet and dry pyrolysis," *Biofuels*, vol. 2, no. 1, pp. 71–106, 2014.
[39] A. A. Peterson, F. Vogel, R. P. Lachance et al., "Thermochemical biofuel production in hydrothermal media: A review of sub- and supercritical water technologies," *Energy Environ. Sci.*, vol. 1, no. 1, pp. 32–65, 2008.
[40] D. Jung, M. Zimmermann, and A. Kruse, "Hydrothermal Carbonization of Fructose: Growth Mechanism and Kinetic Model," *ACS Sustainable Chemistry & Engineering*, vol. 6, no. 11, pp. 13877–13887, 2018.
[41] G. Xu, M. Li, and P. Lu, "Experimental investigation on flow properties of different biomass and torrefied biomass powders," *Biomass and Bioenergy*, vol. 122, pp. 63–75, 2019.
[42] M.-M. Titirici, M. Antonietti, and N. Baccile, "Hydrothermal carbon from biomass: A comparison of the local structure from poly- to monosaccharides and pentoses/hexoses," *Green Chemistry*, vol. 10, no. 11, p. 1204, 2008.
[43] S. Urbonaite, S. Wachtmeister, C. Mirguet et al., "EELS studies of carbide derived carbons," *Carbon*, vol. 45, no. 10, pp. 2047–2053, 2007.
[44] V. Jeanne-Rose, V. Golabkan, J. L. Mansot et al., "An EELS-based study of the effects of pyrolysis on natural carbonaceous materials used for activated charcoal preparation,".
[45] S. D. Berger, D. R. McKenzie, and P. J. Martin, "EELS analysis of vacuum arc-deposited diamond-like films," *Philosophical Magazine Letters*, vol. 57, no. 6, pp. 285–290, 1988.
[46] L. Zhang, X. Yang, F. Zhang et al., "Controlling the effective surface area and pore size distribution of sp2 carbon materials and their impact on the capacitance performance of these materials," *Journal of the American Chemical Society*, vol. 135, no. 15, pp. 5921–5929, 2013.
[47] P. J. Arauzo, L. Du, M. P. Olszewski et al., "Effect of Protein during Hydrothermal Carbonization of Brewer's Spent Grain," *Bioresource Technology*, p. 122117, 2019.
[48] P. Körner, D. Jung, and A. Kruse, "Influence of the pH Value on the Hydrothermal Degradation of Fructose," *ChemistryOpen*, vol. 8, no. 8, pp. 1109–1120, 2019.
[49] J. Köchermann, K. Görsch, B. Wirth et al., "Hydrothermal carbonization: Temperature influence on hydrochar and aqueous phase composition during process water recirculation," *Journal of Environmental Chemical Engineering*, vol. 6, no. 4, pp. 5481–5487, 2018.

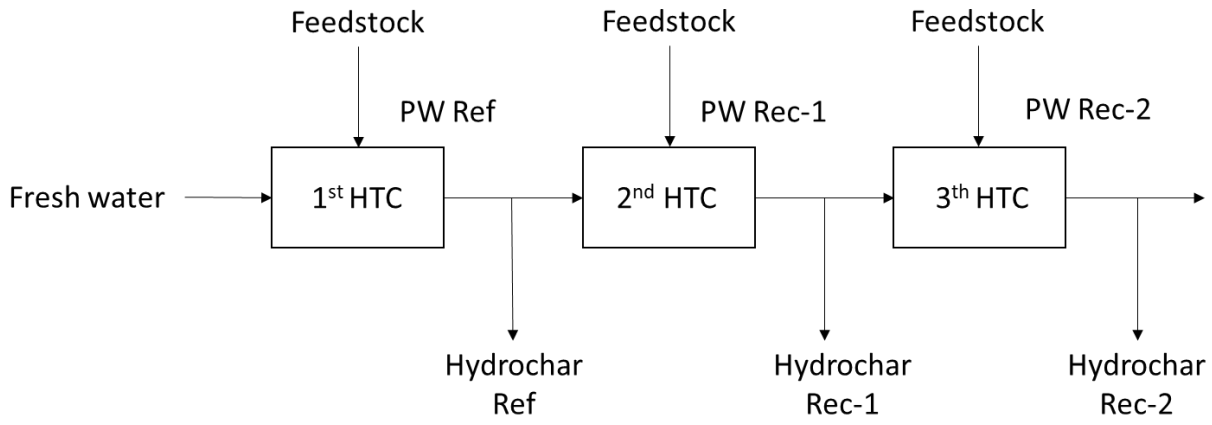

Figure 1. Flow diagram of the process water recirculation for three HTC processes.

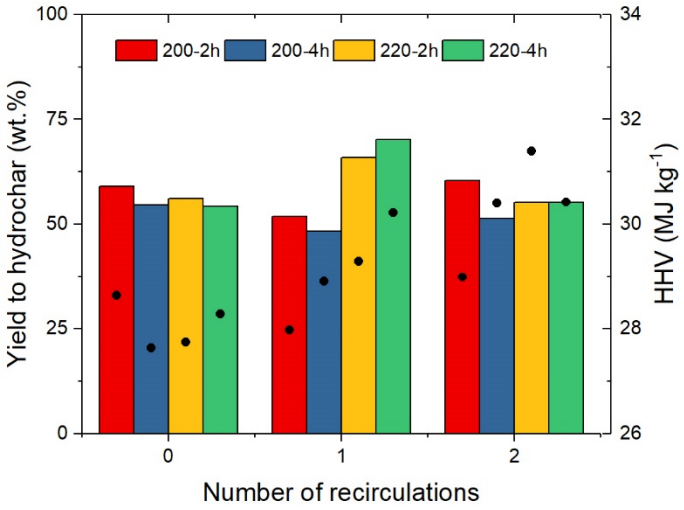

Figure 2. Yield of the hydrochar after HTC (diagram chart) and corresponding HHV (MJ/kg) (black dots).

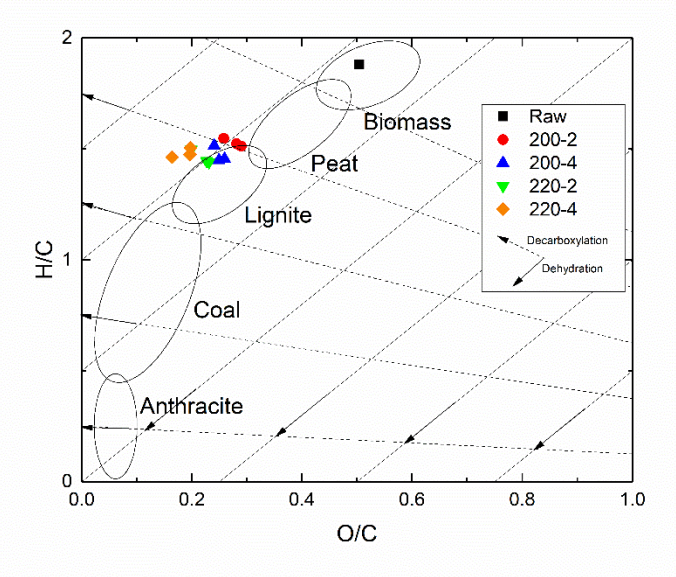

Figure 3. Van Krevelen diagram of the original biomass and produced hydrochars with areas of known coal materials.

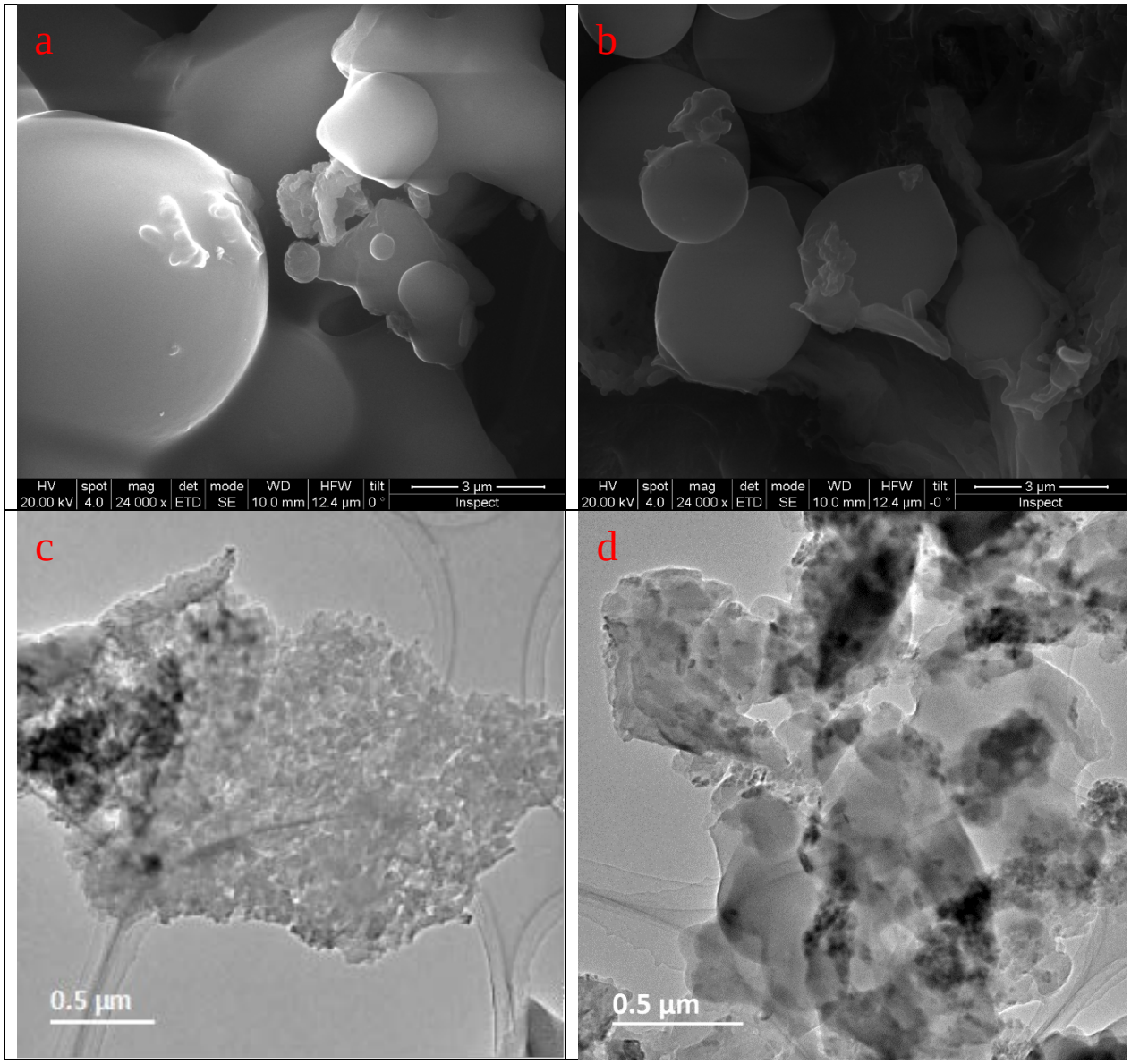

Figure 4. SEM images of produced hydrochars reported at 20.00 kV, a magnification of 24,000x. (a) 220-2h-Ref, (b) 220-2h-Rec-2. TEM images of hydrochars at different operating conditions (c) 220-2h-Ref, (d) 220-2h-Rec-2. All the SEM images and TEM images used on this study are provide at the supplementary material.

Supplementary information for

Assessment of the effects of process water recirculation on the surface chemistry and morphology of hydrochar

P. J. Arauzo1*, M. P. Olszewski[1], X. Wang[2], J. Pfersich[1], V. Sebastian[3], J. Manyà[4], N. Hedin[2], A. Kruse[1]

*Corresponding author, email pabloj.arauzo@uni-hohenheim.de

Address:

[1]Department of Conversion Technologies of Biobased Resources, Institute of Agricultural Engineering, University of Hohenheim, Garbenstrasse 9, 70599 Stuttgart, Germany

[2]Department of Materials and Environmental Chemistry, Stockholm University, SE-10691 Stockholm, Sweden

[3]Department of Chemical Engineering, Aragon Institute of Nanoscience (INA), University of Zaragoza, Campus Río Ebro-Edificio I+D, c/ Poeta Mariano Esquillor s/n, 50018 Zaragoza, Spain

[4]Aragón Institute of Engineering Research (I3A), University of Zaragoza, Crta. Cuarte s/n, Huesca E-22071, Spain

Figure captions

Fig A1. SEM images of produced hydrochars reported at 20.00 kV, a magnification of 24,000x. (a) 200-2h-Ref, (b) 200-2h-Rec-1, (c) 200-2h-Rec-2, (d) 200-4h-Ref, (e) 200-4h-Rec-1, (f) 200-4h-Rec-2, (g) 220-2h-Ref, (h) 220-2h-Rec-1, (i) 220-2h-Rec-2, (j) 220-4h-Ref, (k) 220-4h-Rec-1, (l) 220-4h-Rec-2.

Fig A2. TEM images of hydrochars at different operating conditions (a) 200-2h-Ref, (b) 200-2h-Rec-2, (c) 200-4h-Ref, (d) 200-4h-Rec-2, (e) 220-2h-Ref, (f) 220-2h-Rec-2, (g) 220-4h-Ref, (h) 220-4h-Rec-2.

Fig A3. ^{13}C-NMR spectra of hydrochars hydrothermally carbonized at 220 °C and 220 °C for 2 and 4 hours with fresh water and 2 process water recirculations.

Fig A4. ^{1}H-NMR spectra of hydrochars hydrothermally carbonized at 220 °C and 220 °C for 2 and 4 hours with fresh water and 2 process water recirculations.

Fig A5. Electron energy loss spectroscopy (EELS) spectra in the carbon K-edge region and the π*/σ* intensity ratios for the hydrochars.

Tables

Tab A1. Electron energy loss spectroscopy (EELS) spectra in the carbon K-edge region and the π*/σ* intensity ratios for the hydrochars.

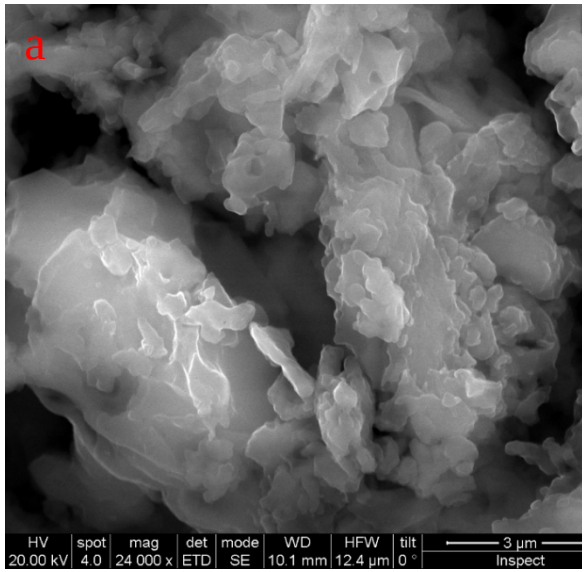
a
HV spot mag det mode WD HFW tilt 3 µm
20.00 kV 4.0 24 000 x ETD SE 10.1 mm 12.4 µm 0 ° Inspect

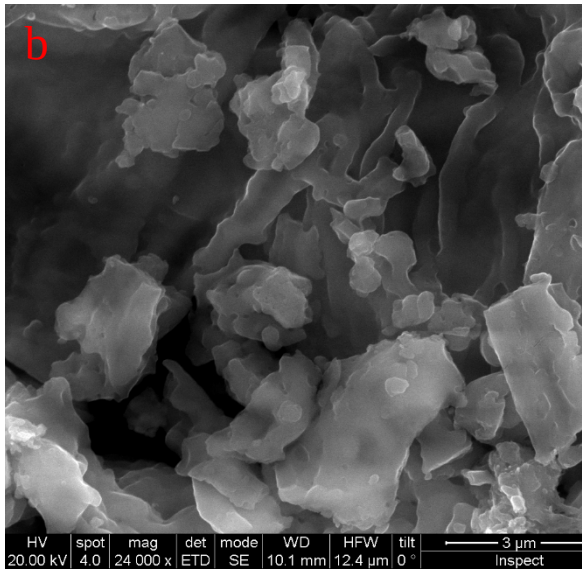
b
HV spot mag det mode WD HFW tilt 3 µm
20.00 kV 4.0 24 000 x ETD SE 10.1 mm 12.4 µm 0 ° Inspect

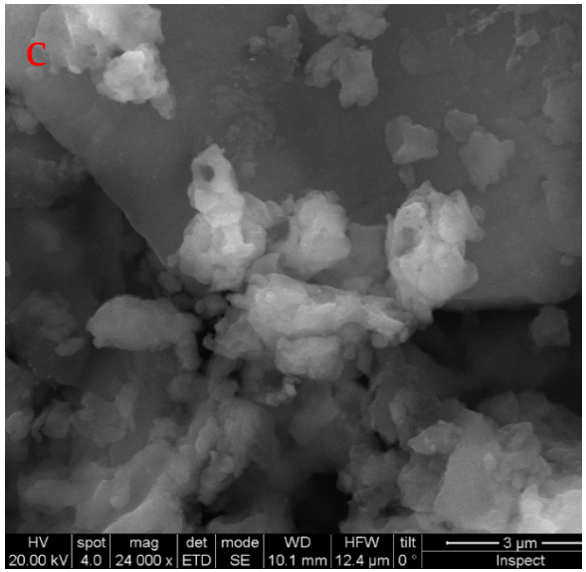
c
HV spot mag det mode WD HFW tilt 3 µm
20.00 kV 4.0 24 000 x ETD SE 10.1 mm 12.4 µm 0 ° Inspect

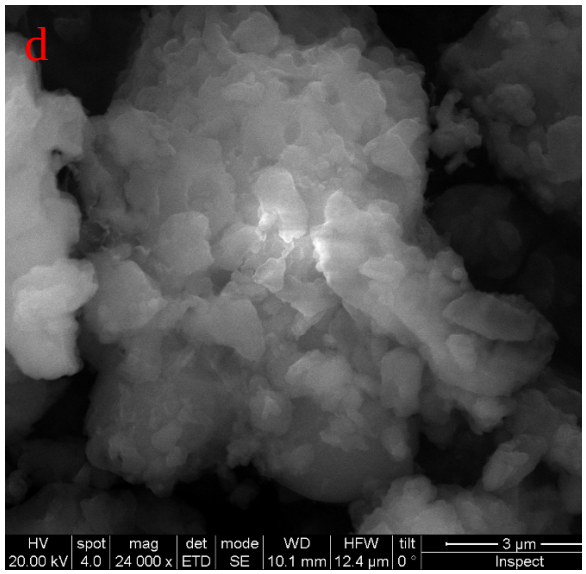
d
HV spot mag det mode WD HFW tilt 3 µm
20.00 kV 4.0 24 000 x ETD SE 10.1 mm 12.4 µm 0 ° Inspect

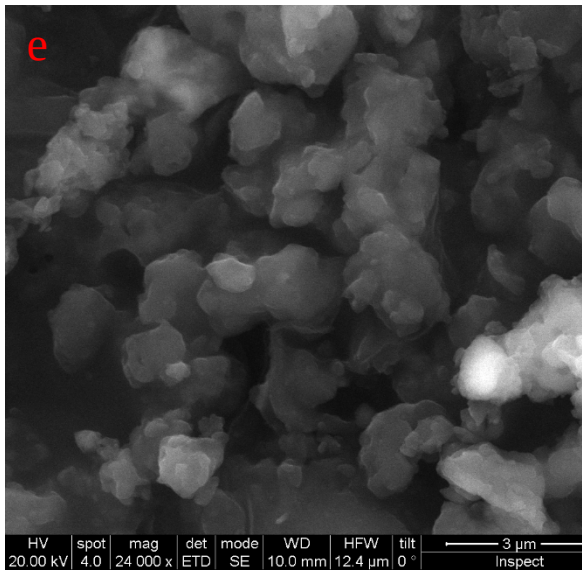
e
HV spot mag det mode WD HFW tilt 3 µm
20.00 kV 4.0 24 000 x ETD SE 10.0 mm 12.4 µm 0 ° Inspect

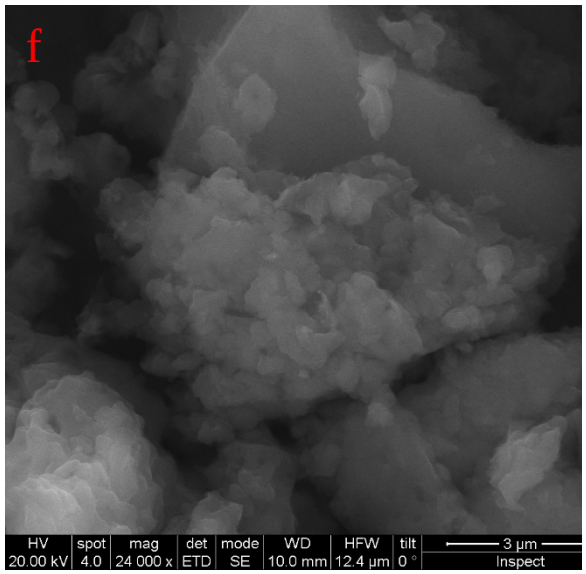
f
HV spot mag det mode WD HFW tilt 3 µm
20.00 kV 4.0 24 000 x ETD SE 10.0 mm 12.4 µm 0 ° Inspect

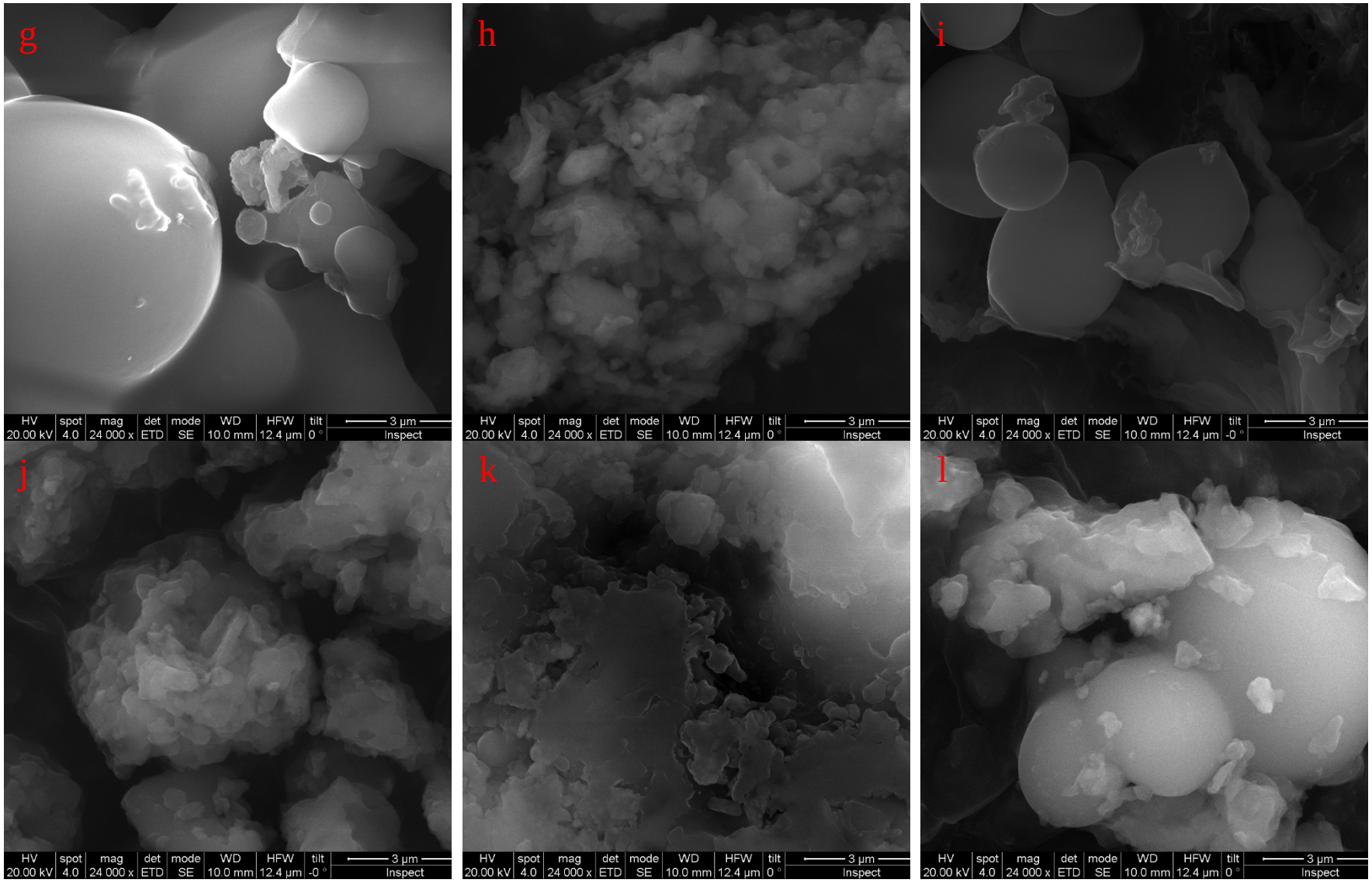
g
HV 20.00 kV | spot 4.0 | mag 24 000 x | det ETD | mode SE | WD 10.0 mm | HFW 12.4 µm | tilt 0 ° | 3 µm | Inspect
h
HV 20.00 kV | spot 4.0 | mag 24 000 x | det ETD | mode SE | WD 10.0 mm | HFW 12.4 µm | tilt 0 ° | 3 µm | Inspect
i
HV 20.00 kV | spot 4.0 | mag 24 000 x | det ETD | mode SE | WD 10.0 mm | HFW 12.4 µm | tilt -0 ° | 3 µm | Inspect
j
HV 20.00 kV | spot 4.0 | mag 24 000 x | det ETD | mode SE | WD 10.0 mm | HFW 12.4 µm | tilt -0 ° | 3 µm | Inspect
k
HV 20.00 kV | spot 4.0 | mag 24 000 x | det ETD | mode SE | WD 10.0 mm | HFW 12.4 µm | tilt 0 ° | 3 µm | Inspect
l
HV 20.00 kV | spot 4.0 | mag 24 000 x | det ETD | mode SE | WD 10.0 mm | HFW 12.4 µm | tilt 0 ° | 3 µm | Inspect

Fig A1. SEM images of produced hydrochars reported at 20.00 kV, a magnification of 24,000x. (a) 200-2h-Ref, (b) 200-2h-Rec-1, (c) 200-2h-Rec-2, (d) 200-4h-Ref, (e) 200-4h-Rec-1, (f) 200-4h-Rec-2, (g) 220-2h-Ref, (h) 220-2h-Rec-1, (i) 220-2h-Rec-2, (j) 220-4h-Ref , (k) 220-4h-Rec-1, (l) 220-4h-Rec-2.

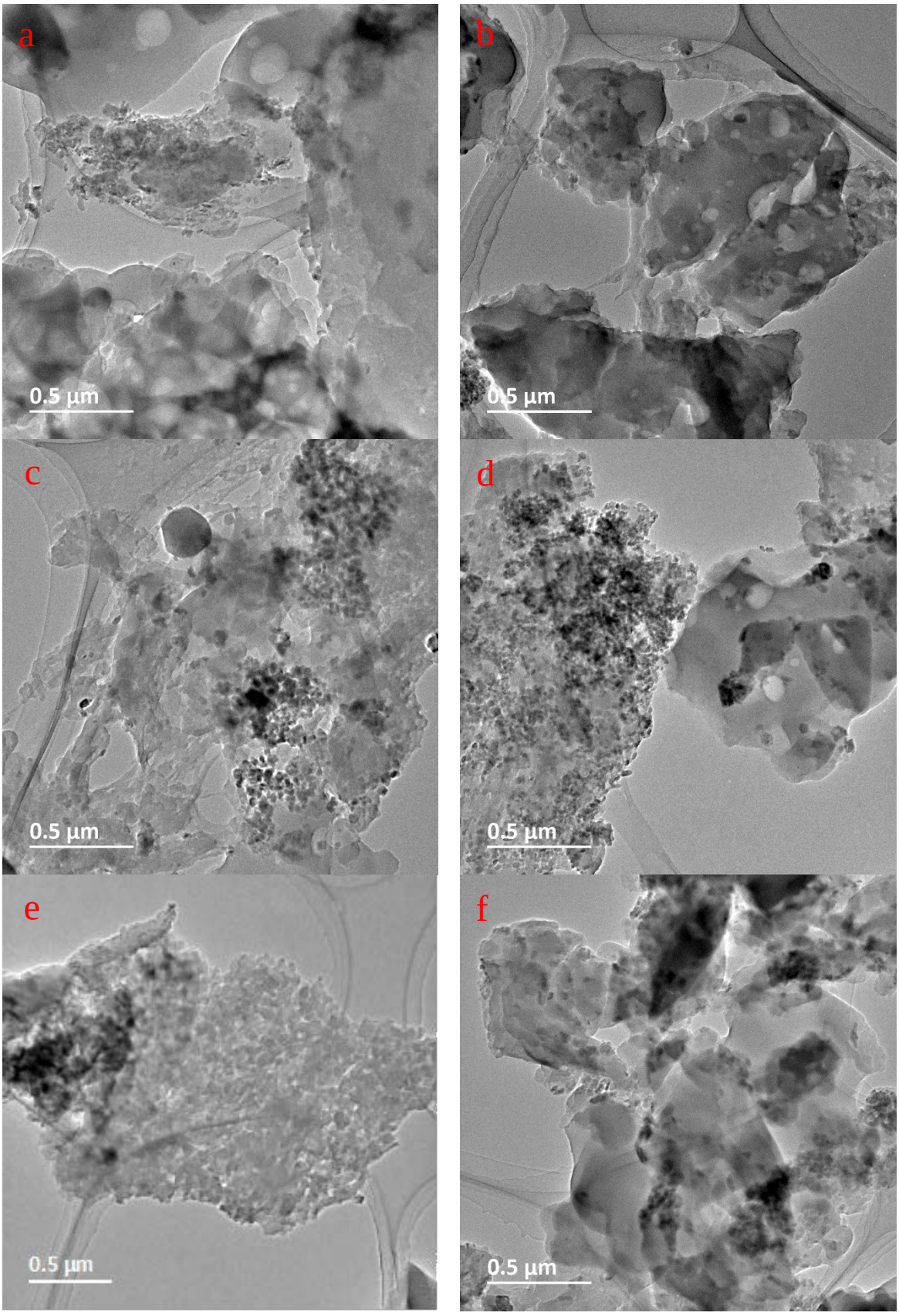
a
0.5 µm
b
0.5 µm
c
0.5 µm
d
0.5 µm
e
0.5 µm
f
0.5 µm

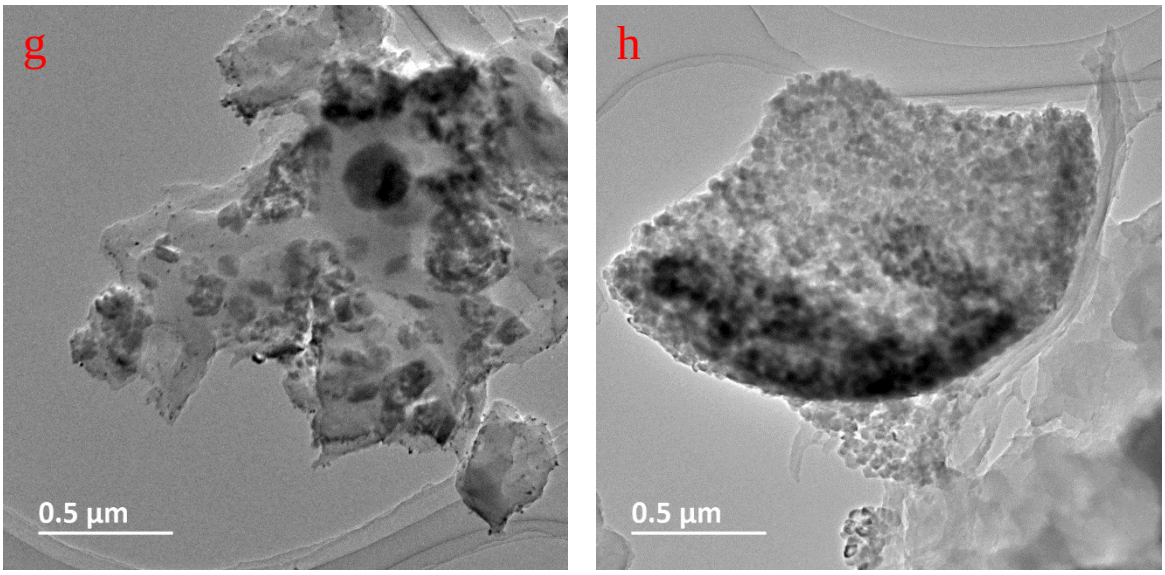

Fig A2. TEM images of hydrochars at different operating conditions (a) 200-2h-Ref, (b) 200-2h-Rec-2, (c) 200-4h-Ref, (d) 200-4h-Rec-2, (e) 220-2h-Ref, (f) 220-2h-Rec-2, (g) 220-4h-Ref, (h) 220-4h-Rec-2.

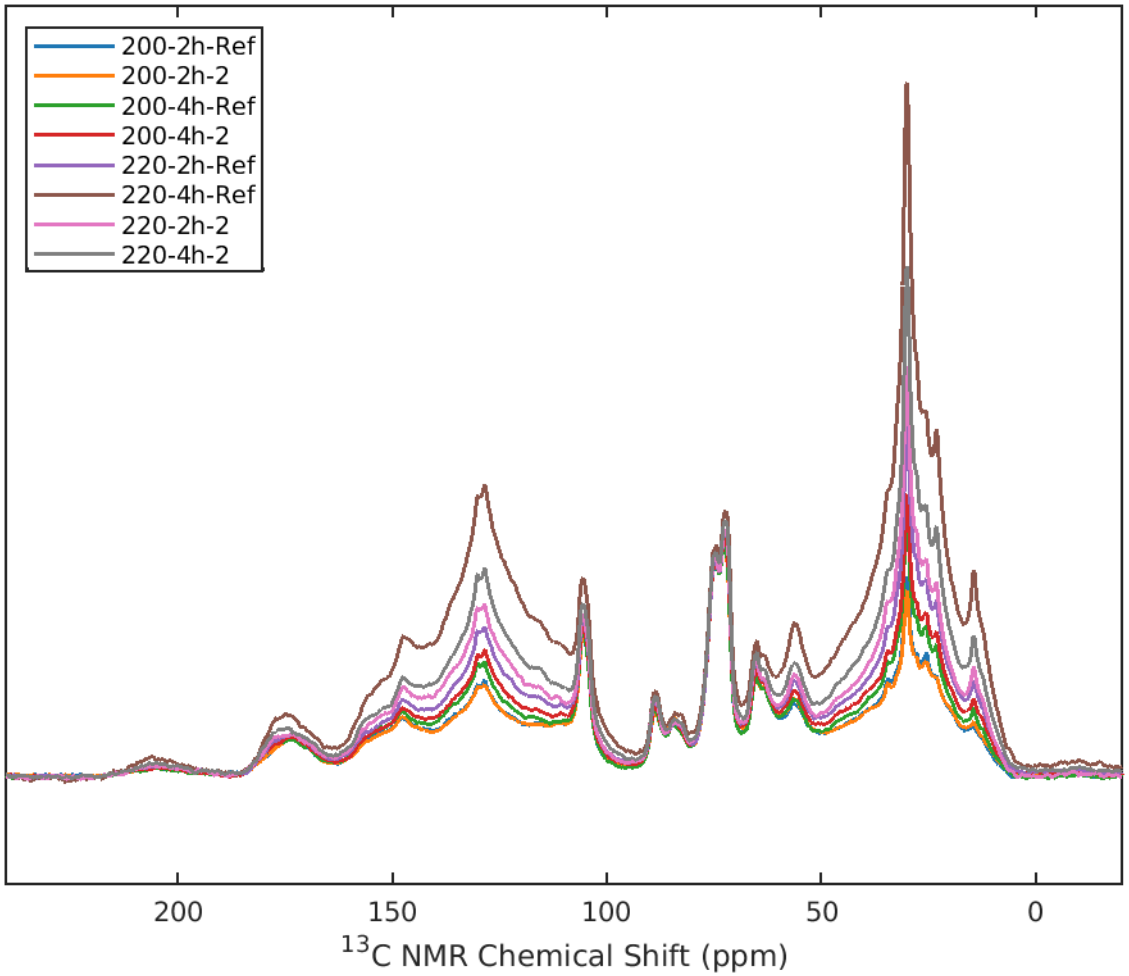

Fig A3. ^{13}C-NMR spectra of hydrochars hydrothermally carbonized at 220 °C and 220 °C for 2 and 4 hours with fresh water and 2 process water recirculations

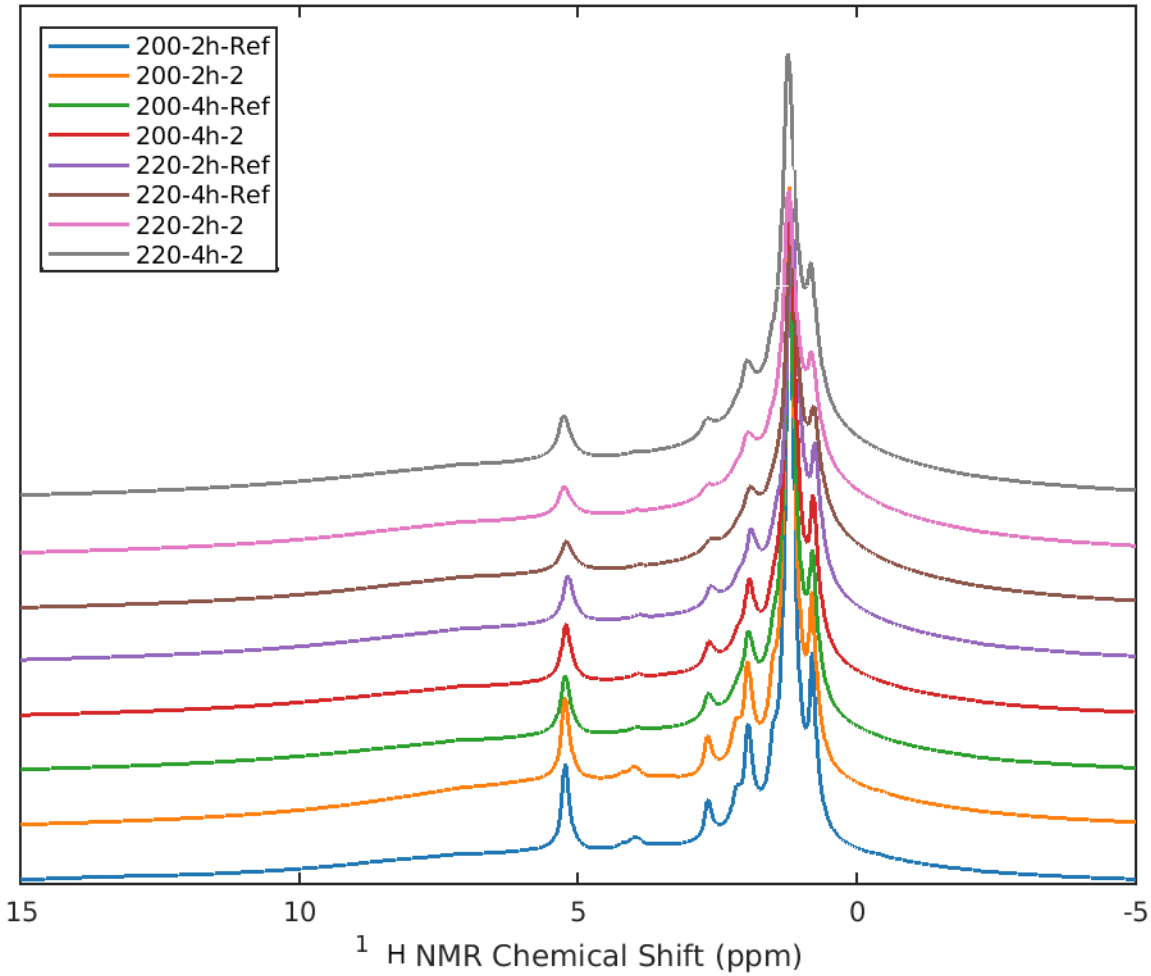

Fig A4. ^{1}H-NMR spectra of hydrochars hydrothermally carbonized at 220 °C and 220 °C for 2 and 4 hours with fresh water and 2 process water recirculations.

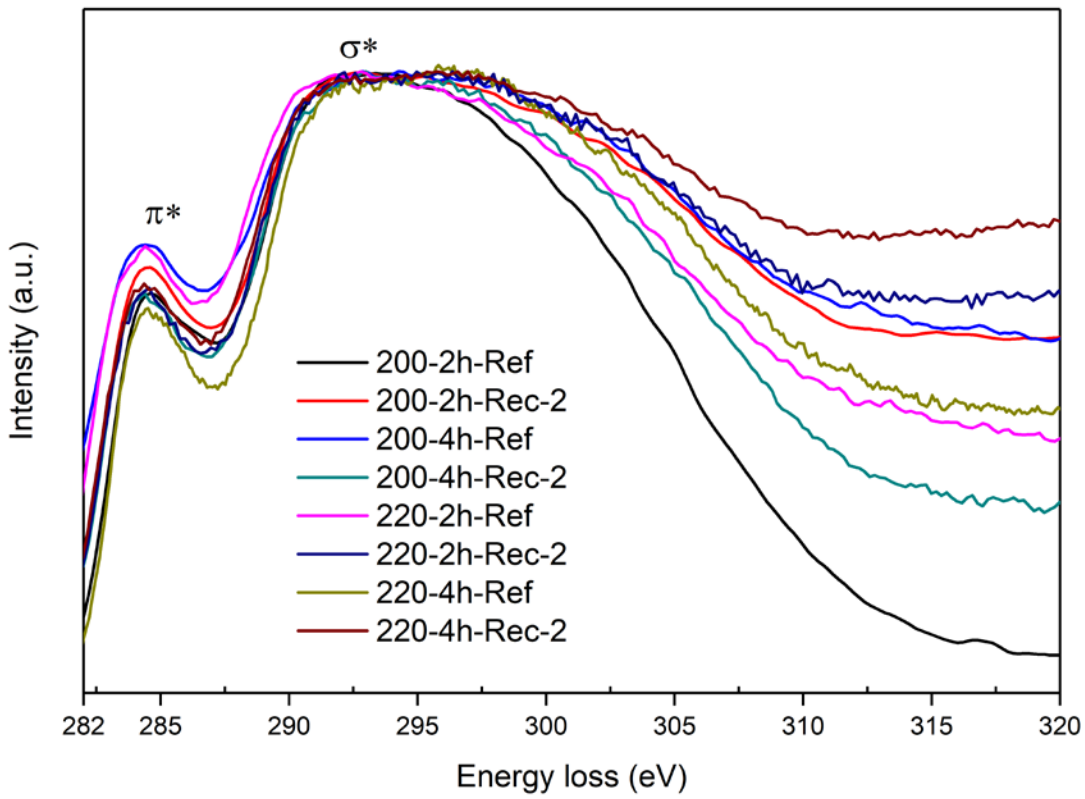

Fig A5. Electron energy loss spectroscopy (EELS) spectra in the carbon K-edge region and the π*/σ* intensity ratios for the hydrochars.

Tab A1. Electron energy loss spectroscopy (EELS) spectra in the carbon K-edge region and the π*/σ* intensity ratios for the hydrochars.

Sample name	$I_{\pi*}/I_{\sigma*}$
200-2h-Ref	0.64
200-2h-Rec-2	0.68
200-4h-Ref	0.72
200-4h-Rec-2	0.64
220-2h-Ref	0.72
220-2h-Rec-2	0.65
220-4h-Ref	0.61
220-4h-Rec-2	0.65